Am J Physiol Endocrinol Metab 310: E624–E632, 2016.
First published January 19, 2016; doi:10.1152/ajpendo.00260.2015.

Changes in one-carbon metabolism after duodenal-jejunal bypass surgery

Jeeyoun Jung,[1,2]* Tae Kyung Ha,[3]* Jueun Lee,[1,5]* Yunmee Lho,[4] Miso Nam,[1,5] Doohae Lee,[1] Carel W. le Roux,[6] Do Hyun Ryu,[5] Eunyoung Ha,[4] and Geum-Sook Hwang[1,7]****

[1]*Integrated Metabolomics Research Group, Seoul Western Center, Korea Basic Science Institute, Seoul, Republic of Korea* [2]*KM Fundamental Research Division, Korea Institute of Oriental Medicine, Daejeon, Republic of Korea;* [3]*Department of Surgery, College of Medicine, Hanyang University, Seoul, Republic of Korea;* [4]*Department of Biochemistry, School of Medicine, Keimyung University, Daegu, Republic of Korea;* [5]*Department of Chemistry, Sungkyunkwan University, Suwon, Republic of Korea;* [6]*Diabetes Complications Research Center, UCD Conway Institute, School of Medicine and Medical Science, University College Dublin, Ireland; and* [7]*Department of Life Science, Ewha Womans University, Seoul, Republic of Korea*

Submitted 5 June 2015; accepted in final form 6 January 2016

Jung J, Ha TK, Lee J, Lho Y, Nam M, Lee D, le Roux CW, Ryu DH, Ha E, Hwang GS. Changes in one-carbon metabolism after duodenal-jejunal bypass surgery. *Am J Physiol Endocrinol Metab* 310: E624–E632, 2016. First published January 19, 2016; doi:10.1152/ajpendo.00260.2015.—Bariatric surgery alleviates obesity and ameliorates glucose tolerance. Using metabolomic and proteomic profiles, we evaluated metabolic changes in serum and liver tissue after duodenal-jejunal bypass (DJB) surgery in rats fed a normal chow diet. We found that the levels of vitamin B_{12} in the sera of DJB rates were decreased. In the liver of DJB rats, betaine-homocysteine *S*-methyltransferase levels were decreased, whereas serine, cystathionine, cysteine, glutathione, cystathionine β-synthase, glutathione *S*-transferase, and aldehyde dehydrogenase levels were increased. These results suggested that DJB surgery enhanced trans-sulfuration and its consecutive reactions such as detoxification and the scavenging activities of reactive oxygen species. In addition, DJB rats showed higher levels of purine metabolites such as ATP, ADP, AMP, and inosine monophosphate. Decreased guanine deaminase, as well as lower levels of hypoxanthine, indicated that DJB surgery limited the purine degradation process. In particular, the AMP/ATP ratio and phosphorylation of AMP-activated protein kinase increased after DJB surgery, which led to enhanced energy production and increased catabolic pathway activity, such as fatty acid oxidation and glucose transport. This study shows that bariatric surgery altered trans-sulfuration and purine metabolism in the liver. Characterization of these mechanisms increases our understanding of the benefits of bariatric surgery.

gastric bypass surgery; metabolomics; proteomics; metabolism

DIABETES AFFECTS ALMOST 10% of the general population and is a leading cause of disability, morbidity, and mortality (15). Although glycemic control and risk factor management have improved, the prevalence of diabetes is still increasing (8, 9). Furthermore, current drug-based therapies for diabetes rarely lead to remission. Thus, there is an urgent need for new therapeutic options.

Bariatric surgery provides a reliable treatment that results in substantial and sustained weight loss in morbidly obese patients and provides a substantial improvement in cases of type 2 diabetes mellitus (T2DM) (5, 6). Bariatric surgery is significantly better than intensive medical therapy for the glycemic control of T2DM at 1–2 years (10, 13, 24, 38). However, the mechanism by which bariatric surgery results in the remission of T2DM remains unclear. Moreover, given that the initial body mass index and postoperative weight loss values are poor predictors of the efficacy of bariatric surgery in patients with diabetes and metabolic syndrome (27, 41), the improvement in glycemia after bariatric surgery is not simply a consequence of sustained weight loss. Therefore, understanding the underlying mechanism of bariatric surgery with respect to the resolution of T2DM is important for the development of more effective and less invasive T2DM therapeutic strategies.

T2DM is multifactorial and includes insulin resistance (4), impaired insulin secretion, and a heterogeneous cluster of environmental and/or hereditary conditions (36). The representative insulin-sensitive tissues are the hypothalamus, adipose tissue, muscle tissue, and liver tissue. The hypothalamus is important for detecting circulating nutrients and hormones in order to maintain energy homeostasis and regulate appetite. When glucose is absorbed into the blood, insulin accelerates glucose uptake into muscle tissue, where it is stored as glycogen or metabolized to produce ATP by glycolysis. Although insulin signaling and glucose metabolism are similar in muscle tissue, excessive consumption of carbohydrates enhances fatty acid synthesis and reduces lipolysis in adipose tissue, suggesting an important relationship between the metabolism of free fatty acid and glucose. Given this, a number of studies have investigated glucose metabolism in these tissues in order to understand their importance in the treatment of obesity and diabetes (25, 33). The liver also plays an important role in metabolism, especially with respect to glucose homeostasis, as it receives signals from nutrients from the intestine as well as from insulin, hormones, and neurotransmitters. The liver is also involved in the synthesis of triglycerides from circulating glucose and fatty acids. Thus, the liver is an important central regulator in the pathogenesis of T2DM (32).

Metabolomic studies provide a powerful analysis of metabolites that reflect the response of biological systems to genetic or environmental changes, whereas proteomic studies provide important information on global protein expression. Gastric bypass surgery influences the effect of microbiota on metabolomic alterations in urine, feces, serum, and circulating branched-chain amino acids (BCAAs) (16, 28, 39, 44). However, no metabolomic studies have been conducted in combination with proteomic studies to investigate the effects of bypass surgery.

We hypothesized that bariatric surgery might induce weight loss-independent alterations in metabolism, which would improve metabolic status after duodenal-jejunal bypass (DJB) surgery, a type of bariatric surgery that excludes the duodenum

* J. Jung, T. K. Ha, and J. Lee contributed equally to this work.
** G.-S. Hwang and E. Ha contributed equally to this work.
Address for reprint requests and other correspondence: G.-S. Hwang: Korea Basic Science Institute, Seoul 120-140, Korea (e-mail: gshwang@kbsi.re.kr).

and proximal jejunum and instead redirects food into the distal jejunum (34). Therefore, we investigated the metabolic changes in serum along with the metabolomic and proteomic profiles in the liver following DJB surgery to examine the mechanisms involved in the improvement of glucose homeostasis after bariatric surgery.

EXPERIMENTAL PROCEDURES

Reagents and chemicals. HPLC-grade water, methanol, and acetonitrile were commercially available (Fisher Scientific). 3-(Trimethylsilyl)-1-propanesulfonic acid-d_6 sodium salt (DSS-d_6, 98 atom %), 3-(trimethylsilyl) propionic-2,2,3,3-d_4 acid sodium salt (TSP, 98 atom %), methanol-d4, chloroform-d4, and deuterium oxide (99.9% vol/vol) were obtained from Cambridge Isotope Laboratories (Andover, MA). All other chemicals and reagents were obtained from Sigma-Aldrich (St. Louis, MO).

Animals and treatments. All experiments were performed in 12-wk-old male Sprague-Dawley (SD) rats (250–300 g) obtained from Central Laboratories (Seoul, Korea) and acclimated for at least 7 days. Rats were group-housed under a controlled temperature (24 ± 1°C) and photoperiod (12:12-h light-dark cycle) and allowed ad libitum access to standard rat chow and tap water. All animal experiments were approved by the Animal Care Committee of Keimyung University, Deagu, Korea, in accordance with the institutional guidelines for care and use of laboratory animals.

DJB operations were initiated by midline incision. The duodenum was ligated with 5-0 silk at the distal edge of the pylorus and the jejunum divided 10 cm beyond the ligament of Treitz. The stomach was created on the greater curvature of the antrum, and a side-to-end gastrojejunostomy was performed with a distal segment of jejunum using 7-0 polydioxanone (PDS) sutures. The open end of the proximal jejunum was anastomosed 15 cm from the gastrojejunal anastomosis in the jejunum using 7-0 PDS sutures. For the sham operations, a midline abdominal incision was performed, and the alimentary circuit of food through the stomach was maintained. Operative time was prolonged to produce a similar degree of anesthetic stress to those mice that underwent DJB. Rats were anesthetized by intraperitoneal injection of zoletil (5–10 mg/kg) and xylazine (10 mg/kg) mixture (1:1).

Rats were fasted overnight before and after surgery, and both groups were fed the same standard chow ad libitum after the operation. Body weight and food intake were measured twice a week for each rat. Rats were euthanized 5 wk after surgery, after which blood and liver tissues were harvested and stored at −80°C.

Sample preparation for metabolomics. For the serum experiment, 270 μl of the serum sample was transferred into the 5-mm outer tube of a two-tube NMR 517 coaxial insert. The inner tube containing DSS-d_6 (98 atom %) was then inserted into the outer tube.

For the liver experiment, 100 mg of liver was transferred to a 1.5-ml tube containing 2.8 mm zirconium oxide beads and homogenized twice at 5,000 rpm with 210 μl of methanol (d_4) and 90 μl of 0.1 M sodium phosphate buffer [in deuterium oxide (D_2O), pH 7.0 ± 0.05] for 20 s using a Precellys 24 tissue grinder (Bertin Technologies, Ampère Montigny-le-Bretonneux, France). After homogenization, 350 μl of methanol (d_4), 150 μl of 0.1 M sodium phosphate buffer (in D_2O, pH 7.0 ± 0.05), and 400 μl of chloroform (d_1) were added to the tube. The mixture was vortexed vigorously for 30 s, allowed to separate for 15 min at 4°C, and centrifuged for 10 min at 13,000 rpm at 4°C. A total of 600 μl of supernatant was removed and mixed with 60 μl of 3-(trimethylsilyl)-propionic-2,2,3,3-d_4 acid sodium salt (TSP, 2.5 mM, 98 atom %) dissolved in 99.9% D_2O. The mixture was then centrifuged for 5 min at 13,000 rpm at 4°C. The supernatants (550 μl) were subsequently transferred into 5-mm NMR tubes (43).

NMR experiments. ^{1}H NMR spectra of serum and liver extracts were acquired on a VNMRS 600 MHz NMR using a triple-resonance, HCN salt-tolerant cold probe (Agilent Technologies, Santa Clara, CA). The pulse sequence used for the serum samples was a CPMG pulse sequence collected into 32K data points with 128 transients, a spectral width of 6,720.430 Hz, relaxation delay of 2.0 s, and an acquisition time of 2.381 s. For the liver extracts, a NOESYPRESAT (RD-90°-t1-90°-tm-90°-FID acquisition) pulse sequence was applied to suppress the residual water signal. A total of 64 transients were collected into 64K data points using a spectral width of 8,445.9 Hz with a relaxation delay of 2.0 s, an acquisition time of 4.00 s, and a mixing time of 100 ms. A 0.5-Hz line broadening function was applied to all spectra prior to Fourier transformation (FT).

NMR data processing for multivariate statistical analysis. The ^{1}H NMR spectra were phased and baseline corrected using Chenomx NMR Suite 7.1 (Chenomx, Edmonton, AB, Canada). The spectral region (δ 0.6–8.5 ppm for serum, δ 0.4–9.8 ppm for liver) of each spectrum was segmented into equal widths (0.005 ppm for serum or liver extracts), and the signal intensities in each spectrum were calculated by integrating these sections. The regions corresponding to water (δ 4.5–5.2 ppm for serum, δ 4.518–5.12 ppm for liver) signal were removed prior to normalization of the spectrum and spectra alignment. The spectra were then normalized to the total spectral area and converted to ASCII format files to perform the alignment using the correlation-optimized warping (COW) method found in MATLAB (R2008a; The Mathworks, Natick, MA).

Multivariate statistical analysis. The processed NMR data were imported to SIMCA-P version 12.0 (Umetrics, Umea, Sweden) and, prior to multivariate data analysis, scaled using the Pareto scaling method, in which each variable was divided by the square root of the standard deviation of the column values. Initially, principal component analysis (PCA) was used as an unsupervised pattern recognition method to examine intrinsic variation in the data set. Next, a partial least squared discriminant analysis (PLS-DA) was performed to minimize the possible contribution of intergroup variability and to further improve separation between the two groups. The quality of the models is described by R^2 and Q^2 values. R^2 was defined as the proportion of variance in the data explained by the models and indicates goodness of fit, and Q^2 is defined as the proportion of variance in the predicted data by the model and indicates predictability.

Targeted metabolite profiling. Targeted profiling of metabolites obtained from ^{1}H NMR spectral data was accomplished using Chenomx NMR Suite 7.1, and glutathione and IMP (inosine monophosphate) were measured by applying multiple-reaction monitoring (MRM) transition using an AB Sciex 6500 liquid chromatography-quadruple linear ion trap mass spectrometer (LC-Q-LIT; AB Sciex, Forest City, CA). Levels of methionine, serine, dimethylglycine (DMG), *S*-adenosylmethionine (SAM), *S*-adenosylhomocysteine (SAH), homocysteine (Hcy), cystathionine, and cysteine were determined on an Agilent 1290 Infinity LC and an Agilent 6490 Triple Quadrupole MS system equipped with an Agilent Jet Stream ESI source (Agilent Technologies).

Protein extraction for proteomics. A total of 100 mg of liver tissue from sham or DJB rats was dissolved in 500-μl sample buffer containing 7 M urea, 2 M thiourea, and 4% (wt/vol) CHAPS. After sonication, the samples were centrifuged at 15,000 rpm and 4°C for 1 h, after which the supernatant was collected. For protein precipitation, 100 μl of supernatant was treated with 10% TCA (vol/vol) and incubated at −20°C for 3 h. The samples were then centrifuged at 15,000 rpm and 4°C for 10 min, and the supernatant was discarded. Protein pellets were lyophilized, dissolved in 500 μl of sample buffer, and centrifuged at 15,000 rpm and 4°C for 30 min. The supernatant was transferred to a new tube and stored at −80°C until further use. Protein concentrations were estimated using a Non-Interfering protein assay kit (Biosciences, St. Louis, MO) according to the manufacturer's instructions.

Two-dimensional electrophoresis experiments, imaging, and identification. In the first dimension, 150 μg of protein extract from each liver sample was applied to an IPG strip (Immobiline DryStrip,

pH 3–10 and pH 4–7, 18 cm; GE Healthcare Life Sciences) for isoelectric focusing (IEF), followed by 200 V for 1 h, 500 V for 30 min, 4,000 V for 30 min, 4,000 V for 1 h, 10,000 V for 1 h, 10,000 V for 13 h, and 50 V for 3 h. The liver protein samples were focused for a total of 110.2 kVh. The strips were equilibrated with 10 mg/ml dithiothreitol in an equilibration buffer for 15 min and then with iodoacetamide for 15 min with continuous shaking. In the second dimension, the equilibrated strips were placed onto 12% SDS-PAGE and run at a constant 20 mA until the dye reached the bottom of the gel. The protein spots in the analytical gels were visualized by silver staining (40).

The gel images were acquired using a BIO-RAD GS-800 scanner and imported into Progenesis SameSpots 2D software (v. 4.1; Nonlinear Dynamics, Newcastle, UK) for analysis. Protein spots with a >2.0-fold ($P < 0.05$) change in abundance or expression were considered differentially expressed. All spots were confirmed visually and edited manually. Differentially expressed proteins were identified using a Mascot-Peptide Mass Fingerprint (www.matrixscience.com) database search.

Western blot, vitamins B_{12} and B_6, and reactive oxygen species. Expressions of betaine-homocysteine methyltransferase (BHMT; Santa Cruz, EU), cystathionine β-synthase (Santa Cruz, EU), glutathione *S*-transferase (Santa Cruz, EU), glucose-6-phosphate dehydrogenase (G6PD; Cell Signaling Technology), phospho-AMPK (Cell Signaling Technology), and β-actin (Sigma) were determined by Western blotting. Rat vitamin B_{12}, B_6, and reactive oxygen species (ROS) levels were measured using ELISA kits (MyBioSource, San Diego, CA) or the OxiSelect ROS/RNS Assay kit (Cell Biolabs, San Diego, CA) according to the manufacturers' instructions.

Statistical analysis. Two-sample *t*-tests, Mann-Whitney tests, Welch *t*-tests, and Spearman's correlation analyses were performed using SAS Statistical Software Package (release 8.02; SAS Institute, Cary, NC) and SPSS 12.0 (SPSS, Chicago, IL). The accepted level of significance was set as $P < 0.05$. Data are presented as means ± SE.

RESULTS

Body weight, food intake, blood glucose level, insulin level, and liver lipid content. Food intake (Fig. 1*A*) and body weight (Fig. 1*B*) did not differ significantly between the sham and DJB rats. However, the blood glucose levels at the onset of the light phase in the DJB group were significantly lower than those in the sham group (Fig. 1*C*). The insulin levels of the sham and DJB groups did not differ significantly (Fig. 1*D*). Additionally, no significant differences in triglyceride ($P = 0.093$) and total cholesterol ($P = 0.078$) liver content in the DJB group were observed after DJB surgery.

Metabolic profiles of sera from sham and DJB rats. The NMR spectra of sera from sham and DJB rats identified 18 sera metabolites (Fig. 2*A*). PLS-DA score plot (Fig. 2*B*) of the global metabolic profiles in the serum showed a different pattern of metabolism between sham controls and DJB rats [R^2X: 71.7%, R^2Y: 92.0%, Q^2: 71.5% in serum model (sham controls $n = 7$; DJB rats $n = 8$)]; the reliability of the PLS-DA models was validated using a 100-fold repeated permutation test (Fig. 2*B*). We observed that the levels of formate, glutamine, succinate, and lactate in the serum were significantly altered after DJB surgery ($P < 0.05$, Fig. 2*C*).

Metabolic profiles of livers from sham and DJB rats. NMR spectra of liver tissue from sham and DJB rats contained 33 hepatic metabolites (Fig. 3*A*). PLS-DA score plot (Fig. 3*B*) of the global metabolic profiles in livers acquired using NMR spectrometry showed a different pattern of metabolism between sham controls and DJB rats [R^2X: 50.8%, R^2Y: 94.4%, Q^2: 84.0% in liver model (sham controls $n = 7$; DJB rats $n = 9$)], and the reliability of the PLS-DA models was validated using a 100-fold repeated permutation test (Fig. 3*B*). The levels of ADP, AMP, ATP, alanine, choline, formate, glutamine, hypoxanthine, isoleucine, lactate, NADP+, pyruvate, succinate, and valine in the liver samples significantly differed between the groups ($P < 0.05$; Fig. 3*C*).

Correlation analyses of serum and liver metabolites. Spearman's correlation analyses were applied to assess the associations between serum and liver metabolites that were significantly changed between sham and DJB rats (Fig. 4). Serum formate was the highest correlated metabolite with

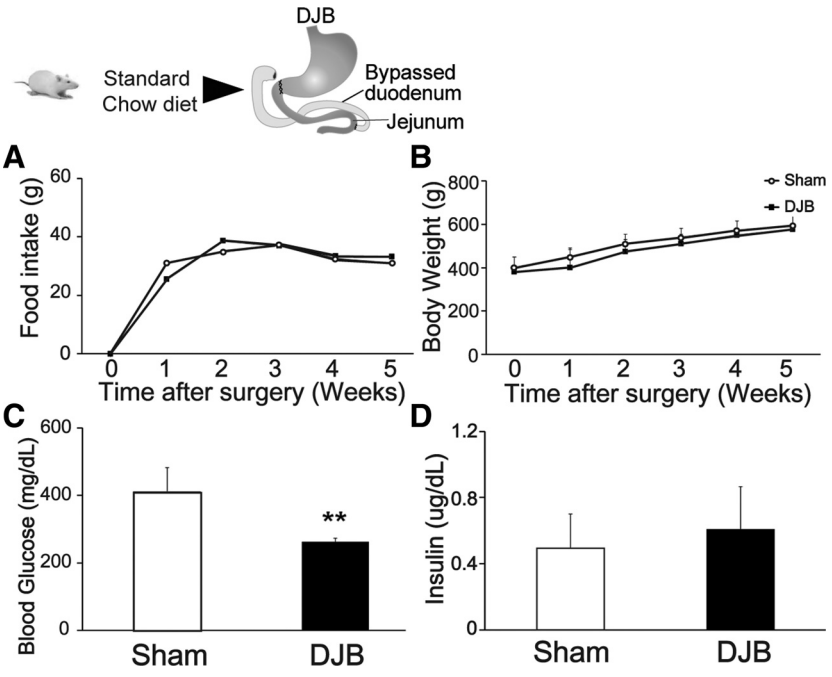

Fig. 1. Changes in food intake, body weight, blood glucose levels, and insulin levels between the sham and duodenal-jejunal bypass surgery (DJB) groups. No significant differences in food intake (*A*) and body weight (*B*) were observed. Blood glucose levels (*C*) of the DJB group were significantly lower than those of the sham group, and no significant differences in insulin levels (*D*) between the sham and DJB groups were observed (**$P < 0.01$).

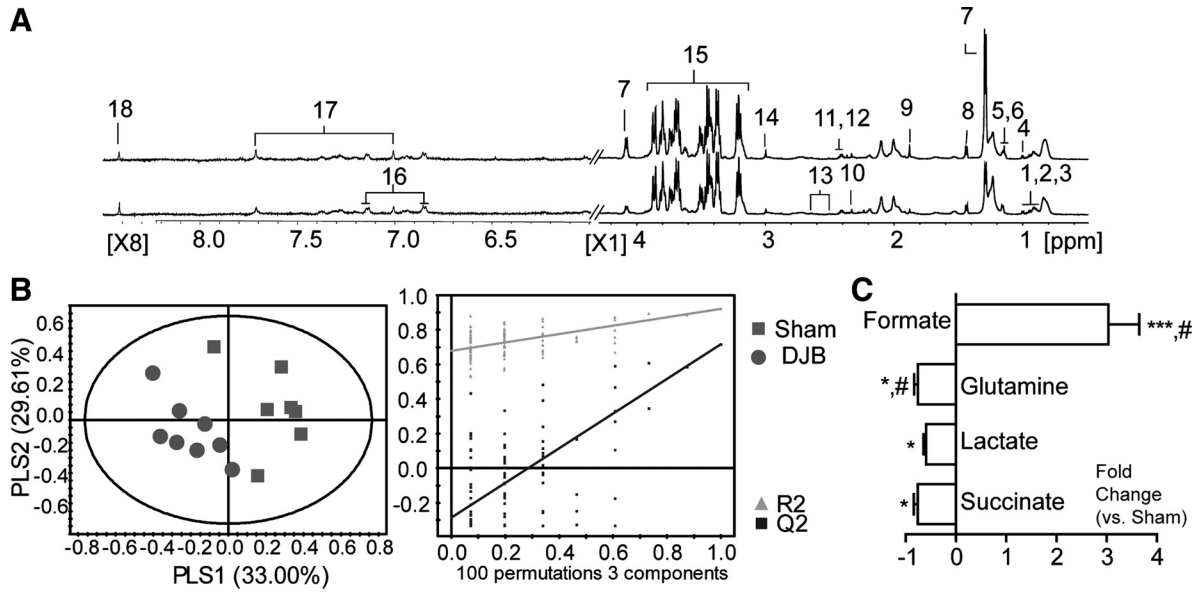

Fig. 2. Metabolic profiles of sera from sham and DJB rats using NMR spectroscopy. *A*: representative 1H-NMR spectra of sera from sham control (*up*) and DJB rats (*down*) (R^2X = 84.6%, $Q2$ = 51.2%). Key: 1, leucine; 2, isoleucine; 3, 2-hydroxybutyrate; 4, valine; 5, propylene glycol; 6, 3-hydroxybutyrate; 7, lactate; 8, alanine; 9, acetate; 10, pyruvate; 11, glutamine; 12, succinate; 13, citrate; 14, creatine; 15, glucose; 16, tyrosine; 17, histidine; 18, formate. *B*: score (*left*) and permutation (*right*) plots of partial least squares-discriminant analyses (PLS-DA) of sera [R^2X: 71.7%, R^2Y: 92.0%, $Q2$: 71.5% in the serum model (sham controls n = 7 and DJB rats n = 8)]. *C*: quantitative fold changes of significantly altered sera metabolites. *$P < 0.05$, **$P < 0.01$, ***$P < 0.001$; # and †, Mann-Whitney test and Welch *t*-test, respectively.

liver metabolites such as ADP, AMP, ATP, alanine, choline, hypoxanthine, isoleucine, lactate, NADP+, pyruvate, and succinate. Serum glutamine was associated with the presence of isoleucine and pyruvate in the liver. Serum lactate was also strongly correlated with a number of liver metabolites, including ADP, alanine, choline, formate, glutamate, hypoxanthine, isoleucine, pyruvate, and succinate. Finally, serum levels of succinate were positively correlated with those of formate, glutamate, hypoxanthine, and pyruvate in liver.

Proteomic analysis of liver samples from sham and DJB rats. The 2D gel images of proteins extracted from the livers of the sham (n = 3) and DJB groups (n = 3) were analyzed using computational methods (Fig. 5*A*). The seven identified proteins, namely, aldehyde dehydrogenase, microtubule-actin cross-linking factor 1, ATP-dependent zinc metalloprotease YME1L1, H(+)-transporting ATP synthase, delta-aminolevulinic acid dehydratase, guanine deaminase, and IMP showed over 2.0-fold changes (increase or decrease) in their relative abundance, with a P value of <0.05 in a *t*-test between the two groups; thus, their expression significantly differed (Fig. 5*B*).

Trans-methylation and trans-sulfuration pathway. Our NMR-based metabolic profiling identified a strong correlation between various serum and liver metabolites. In particular, high levels of circulating formate were associated with the liver metabolites ADP, AMP, ATP, and hypoxanthine, which are intermediates in purine metabolism, an output of one-carbon metabolism (45). In addition, previous studies (17, 18) had suggested that elevated levels of formate in plasma could be related to altered cellular one-carbon metabolism. Thus, we measured the concentrations of vitamin B_{12} and vitamin B_6, which affect the trans-methylation (remethylation process) and trans-sulfuration pathways, respectively. The concentration of vitamin B_{12} in the serum from the DJB group was significantly lower than that from the sham control group, but the concentrations of vitamin B_6 from the control and DJB groups did not differ significantly (Fig. 6, *A* and *B*). However, the plasma total Hcy was decreased in DJB rats (Fig. 6*C*). Thus, we further investigated one-carbon metabolism in the liver after DJB surgery.

In the liver, the expression level of BHMT, which transfers a methyl group to a Hcy via the demethylation of betaine to generate dimethylglycine, was decreased in the DJB group compared with the sham controls (Fig. 6*D*). However, one-carbon metabolites affecting trans-methylation, such as choline, betaine, DMG, methionine, *S*-adenosylmethionine (SAM), *S*-adenosylhomocysteine (SAH), and Hcy, did not significantly differ in the groups receiving normal chow (Fig. 6*E*).

We observed significantly increased levels of serine, cystathionine, cysteine, and glutathione (Fig. 6*E*), accompanied by an increased expression of cystathionine β-synthase (CBS; Fig. 6*D*), glutathione *S*-transferase (GST; Fig. 6*D*), and aldehyde dehydrogenase in the livers of the DJB group. These results suggest that DJB increased the trans-sulfuration and its consecutive processes such as detoxification and the scavenging activities of ROS. Thus, we measured the level of ROS in the liver using the fluorescent dye 2′,7′-dichlorodihydrofluorescein (DCF) and observed significantly decreased levels of DCF fluorescence in the DJB group (Fig. 6*F*).

Purine pathway. In the liver, DJB rats showed increased levels of purine metabolites (ATP, ADP, and AMP) and the first fully formed purine IMP (Fig. 7*A*).

Purine de novo synthesis started with phosphoribosyl pyrophosphate (PRPP), which is produced primarily through the pentose phosphate pathway. To determine the activity of the pentose phosphate pathway, we observed the levels of phospho*enol*pyruvate carboxykinase-1 (PEPCK1), glucose-

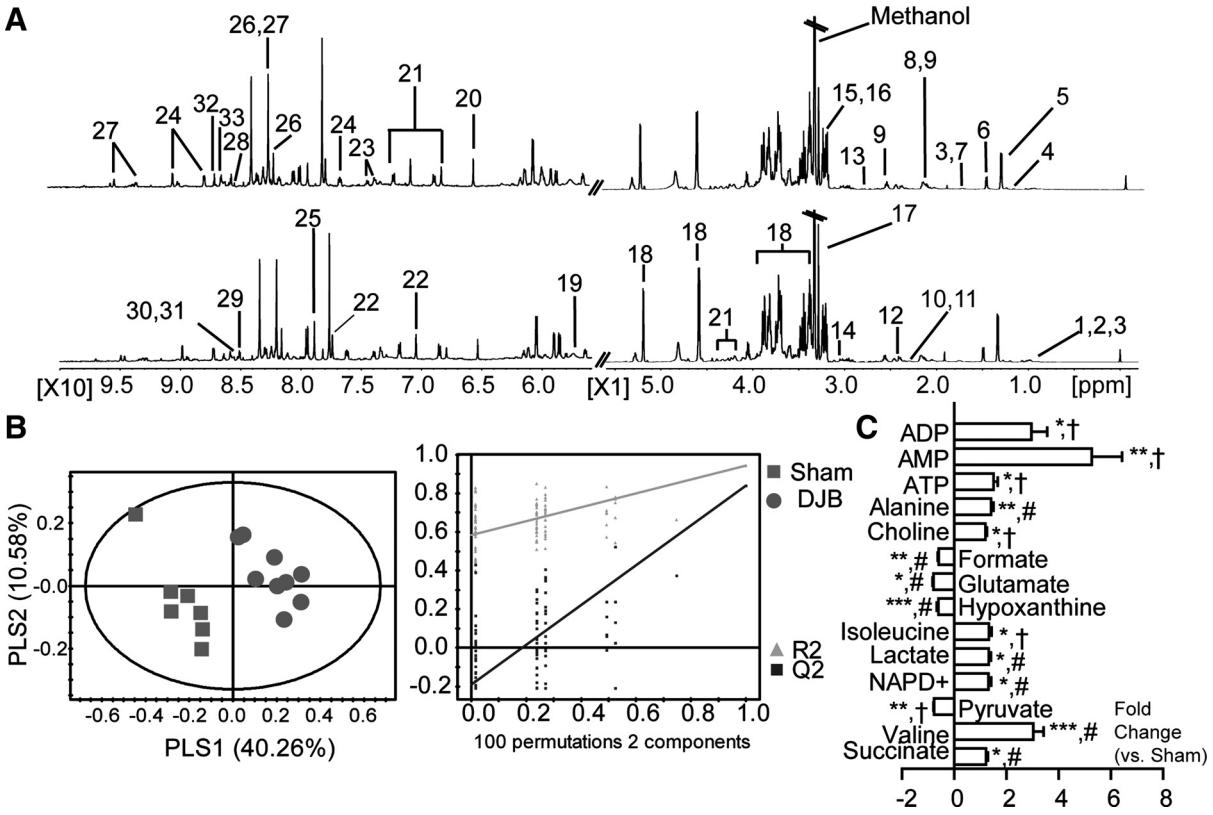

Fig. 3. Metabolic profiles using NMR spectroscopy of livers from sham and DJB rats. *A*: representative 1H-NMR spectra of the liver from sham control (*up*) and DJB rats (*down*) Key: 1, valine; 2, isoleucine; 3, leucine; 4, 3-hydroxybutyrate; 5, lactate; 6, alanine; 7, lysine; 8, glutamate; 9, glutamine; 10, malate; 11, pyruvate; 12, succinate; 13, dimethylamine; 14, creatine; 15, choline; 16, O-phosphocholine; 17, betaine; 18, glucose; 19, urea; 20, fumarate; 21, tyrosine; 22, histidine; 23, phenylalanine; 24, nicotinamide; 25, NAD+; 26, hypoxanthine; 27, NADP+; 28, formate; 29, ADP; 30, NADH; 31, NADPH; 32, AMP; 33, ATP. *B*: score (*left*) and permutation (*right*) plots of PLS-DA of liver [R^2X: 50.8%, R^2Y: 94.4%, $Q2$: 84.0% in the liver model (sham controls $n = 7$ and DJB rats $n = 9$)]. *C*: quantitative fold changes of significantly altered hepatic metabolites. $^*P < 0.05$, $^{**}P < 0.01$, $^{***}P < 0.001$; # and † Mann-Whitney test and Welch *t*-test, respectively.

6-phosphate phosphatase (G6PC), and G6PD. Expression of G6PC and G6PD were decreased and increased, respectively, in DJB rats (Fig. 7, *B* and *C*). Levels of NADP+ also increased in DJB rats compared with sham controls. In addition, both a significant increase in lactate, alanine, and BCAAs (isoleucine and valine) and a decrease in ATP/ADP ratio (Fig. 7*D*) in the liver were observed. These results were indicative of an enhanced pentose phosphate pathway and reduced gluconeogenesis in DJB rats (35).

In contrast to the increased purine synthesis pathway, proteomics analysis of the liver revealed decreased levels of guanine deaminase, an enzyme involved in GTP degradation, and lower levels of hypoxanthine, a metabolite of purine degradation, both of which are associated with reduced purine degradation. In particular, altered purine metabolism affects the energy-regulating system by altering the AMP/ATP ratio, which is used by the cell to sense how much energy is available. An increased AMP/ATP ratio results in enhanced energy production and catabolic activity, such as fatty acid oxidation and glucose transport, by activating AMPK expression. On the basis of our results, DJB rats showed a 3.17-fold higher AMP/ATP ratio than that shown by the sham controls ($P < 0.001$; Fig. 7*E*). In addition, AMPK phosphorylation was increased in the DJB rats compared with that in the sham controls (Fig. 7*F*).

DISCUSSION

In this study, an established rat model of DJB surgery revealed metabolic changes in serum and liver samples as determined by an integrated metabolomic and proteomic investigation. Formate levels in sera, a novel window into cellular one-carbon metabolism, increased and vitamin B_{12} decreased in DJB rats (18). In addition, we found that DJB rats fed normal chow diets showed significantly lower levels of plasma Hcy, which was inconsistent with general vitamin B_{12} deficiency status (20, 21). Thus, we further investigated the altered one-carbon metabolism in the liver.

Three pathways are involved in the removal of Hcy. First, Hcy can be remethylated into methionine through the activity of methionine synthase (MS) when there is sufficient folic acid and vitamin B_{12} or through the activity of liver-specific BHMT. Alternatively, Hcy can be irreversibly converted into cysteine through trans-sulfuration. In the current study, BHMT showed slightly reduced expression in the liver of DJB rats. In addition, metabolites and proteins related to the trans-sulfuration pathway were increased, which suggests that DJB surgery may accelerate the Hcy-dependent trans-sulfuration pathway rather than trans-methylation, resulting in lower levels of plasma Hcy in DJB rats fed a normal chow diet.

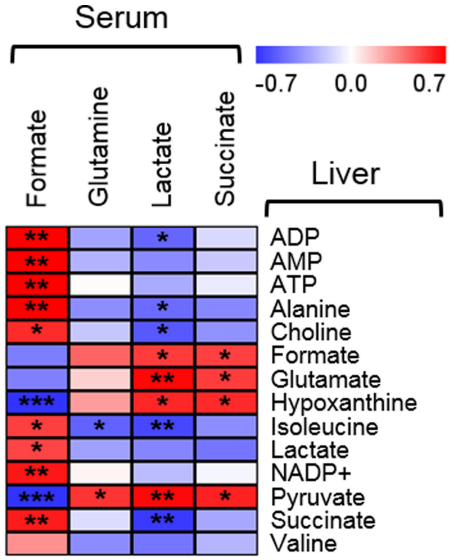

Fig. 4. Correlation analyses between serum and liver metabolites. Each square represents the Spearman's correlation coefficient between serum and liver metabolites measured by NMR spectroscopy. Red and blue indicate positive and negative correlation, respectively (range in value from −0.7 to +0.7). *$P < 0.05$, **$P < 0.01$, ***$P < 0.001$.

Trans-sulfuration is favored with the upregulation of CBS. Several studies have reported that increased trans-sulfuration resulted in higher levels of cysteine, which can serve as a substrate for gluconeogenesis via its conversion to pyruvate, leading to hyperglycemia (14, 29, 37). However, we observed that random glucose levels were lower in the DJB group than in the control group.

Gluconeogenesis in the liver occurs from carbon precursors such as lactate, alanine, and glycerol, and these processes are ATP dependent (19). In the current study, we observed an increase in lactate, alanine, and BCAA levels and a decrease in both pyruvate and the ATP/ADP ratio in the liver after DJB surgery. A low ATP/ADP ratio reflects the inactivation of pyruvate kinase, resulting in reduced levels of hepatic pyruvate and gluconeogenesis (1). Further studies showed that G6PC, the rate-limiting enzyme that dephosphorylates glucose 6-phosphate into glucose in gluconeogenesis, was reduced in DJB rats, which may explain the lower glucose level in the DJB group.

In addition, DJB surgery enhanced the consecutive reactions of trans-sulfuration. We observed increased levels of CBS, GST, and glutathione in the DJB group. GST and glutathione play important roles in the process of detoxification (26, 31). These proteins detoxify 4-hydroxynonenal and 4-hydroxyhexenal, the toxic end-products of lipid peroxidation, by conjugating aldehyde dehydrogenase to GST-catalyzed glutathione (12). Bell et al. (2) also reported that DJB surgery reduced the hepatic malondialdehyde (MDA) levels (a marker of lipid peroxidation), and levels of ROS of DJB were decreased in this study. In particular, it is worth noting that these results did not come from weight loss, and we also found no significant difference in triglyceride and total cholesterol levels in the liver between the sham controls and the DJB group, because we used a normolipidemic animal model fed a normal chow diet.

However, we observed that the expression of BHMT was slightly decreased in the DJB group. This result was unexpected, as we initially hypothesized that a reduced vitamin B_{12} level and consequent reduction in vitamin B_{12}-dependent MS activity would be compensated for by an increased level of BHMT. This result is suggestive of another as yet unidentified regulatory mechanism of BHMT by DJB or may indicate that the degree of reduced activity in vitamin B_{12}-dependent MS was not sufficient to be compensated for by the increase in BHMT activity.

Instead, serine was significantly increased in DJB rats. Serine synthesis from glycine and methionine synthesis via the remethylation of Hcy are two processes that represent alternative uses of the one-carbon group of 5,10-methylene-tetrahydrofolate (THF). Cuskelly et al. (7) reported that 10-methylene-THF is directed toward serine synthesis under a reduced rate of methionine synthesis.

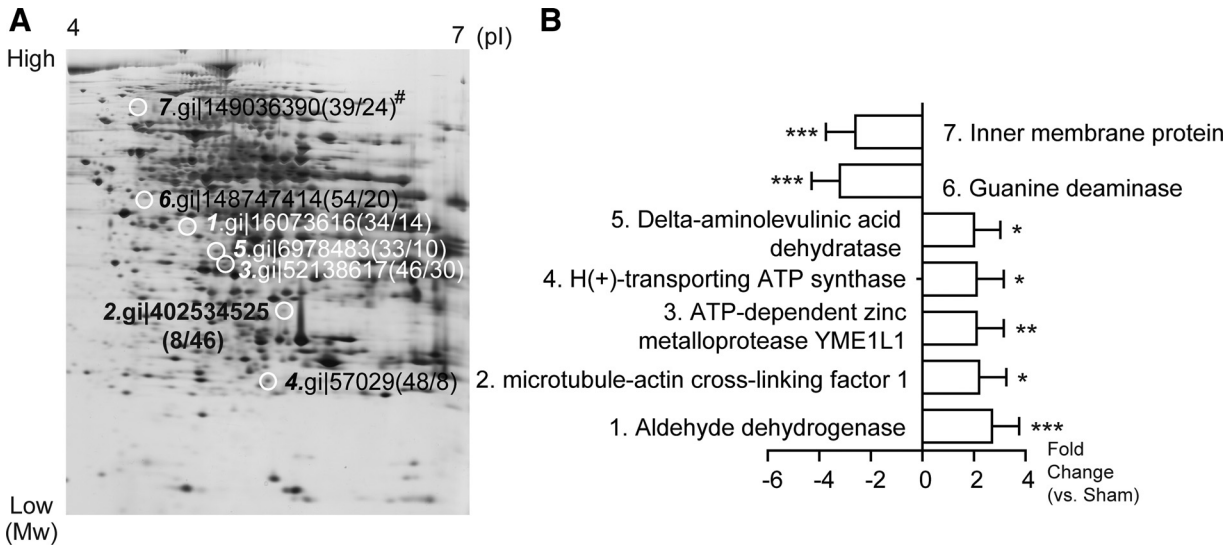

Fig. 5. Proteomics approach to livers from sham and DJB rats. *A*: representative 2D gel image of a liver; keys indicate 7 significantly altered proteins; #accession no. [sequence coverage (%)/peptides matched]. *B*: fold changes of significantly altered hepatic proteins in abundance. *$P < 0.05$, **$P < 0.01$, ***$P < 0.001$.

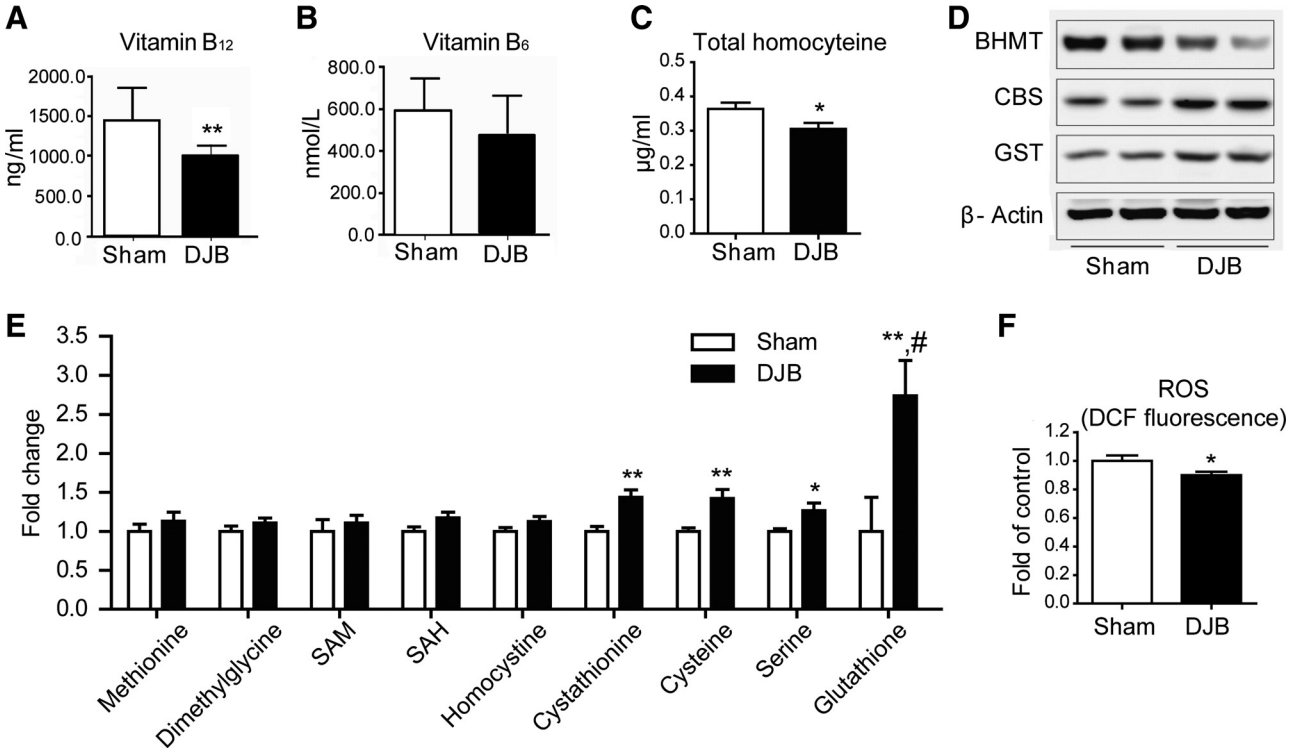

Fig. 6. Altered trans-methylation and trans-sulfuration pathway. *A–C*: vitamin B_{12} (*A*), B_6 (*B*), and total homocysteine (*C*) levels in the blood. *D*: Western blot analysis of betaine-homocysteine *S*-methyltransferase (BHMT), cystathionine β-synthase (CBS), and glutathione *S*-transferase (GST). *E*: changes in hepatic metabolites associated with the trans-methylation and trans-sulfuration pathway detected by LC-MS. SAM, *S*-adenosyl methionine; SAH, *S*-adenosyl homocysteine. Data are expressed as means ± SE. $*P < 0.05$, $**P < 0.01$, $***P < 0.001$; #Mann-Whitney test. *F*: intensity of DCF fluorescence [indicator for reactive oxygen species (ROS)] between sham controls and DJB rats ($*P < 0.05$, $**P < 0.01$, $***P < 0.001$).

In the current study, we observed higher levels of purine metabolites such as ATP, AMP, and ADP in DJB rats. Reduced levels of G6PC in DJB rats could provide PRPP by shifting the flow of glucose 6-phosphate to the pentose phosphate pathway (PPP) (35). In addition, increased levels of G6PD, the first rate-limiting enzyme of PPP oxidizing glucose 6-phosphate into 6-phospho-glucono-1,5-lactone, were indicative results of enhancement of PPP in rats after DJB surgery. NADP+, the most important regulatory factor of the PPP, and the first fully formed purine, IMP, were also increased in DJB rats (3). These results showed that DJB surgery enhanced purine de novo synthesis by altering the one-carbon cycle.

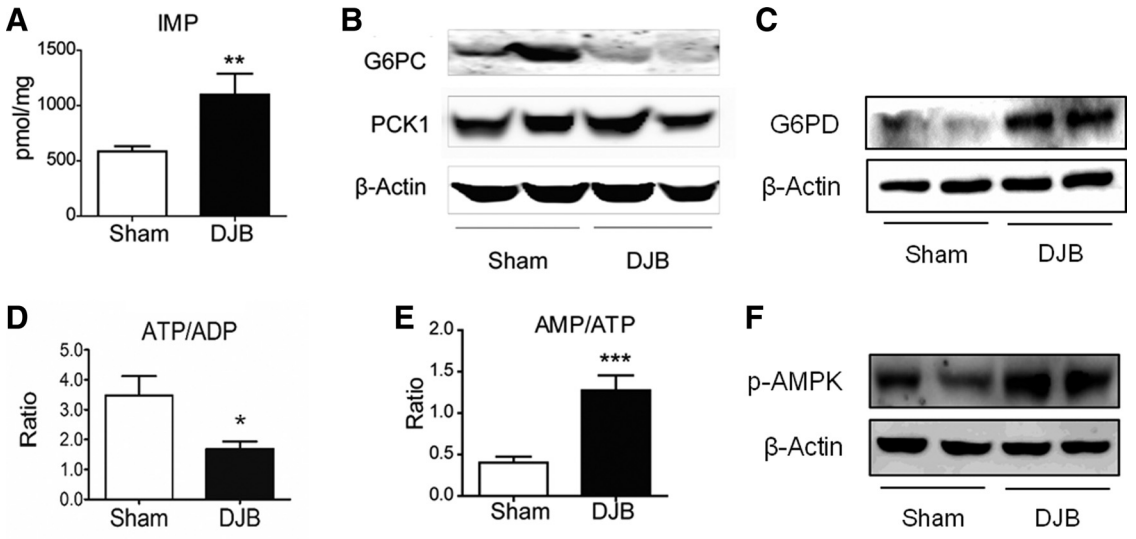

Fig. 7. Increased energy production and catabolic pathway activity. *A*: level of inosine monophosphate (IMP) detected using liquid chromatography-quadrupole linear ion trap mass spectrometry (LC-Q-LIT). *B* and *C*: Western blot analysis of glucose-6-phosphate phosphatase (G6PC) and phospho*enol*pyruvate carboxykinase (PCK1; *B*) and glucose-6-phosphate dehydrogenase (G6PD; *C*). *D* and *E*: ATP/ADP ratio (*D*) and AMT/ATP ratio (*E*) between sham controls and DJB rats; $*P < 0.05$, $**P < 0.01$, $***P < 0.001$. *F*: Western blot analysis of phospho-AMPK of sham and DJB rats.

In contrast to the increased purine synthesis, DJB rats showed lower hypoxanthine, an intermediate metabolite in the purine degradation pathway, and guanine deaminase, an enzyme involved in the purine degradation pathway, levels, indicating that the degradation rate of purine metabolites decreased after DJB surgery. The decreased purine catabolic pathway may have also contributed to the reduced ROS levels in the DJB group, because conversion of hypoxanthine and xanthine into uric acid by xanthine oxidase generates a significant amount of ROS (42).

The altered purine metabolism may have also caused the change in the AMP/ATP ratio in DJB rats (22, 23). Indeed, we observed an increased AMP/ATP ratio in the DJB group in the current study. A higher AMP/ATP ratio activates AMP-activated kinase, which results in increased utilization of energy fuels such as glucose and fatty acids (11, 30).

Here, we demonstrate for the first time (using a multi-omics study) enhanced trans-sulfuration and altered purine metabolism after DJB surgery, which may contribute to the therapeutic effects of bypass surgery. These findings increase our understanding of the mechanisms that underlie the metabolic improvements achieved after DJB.

GRANTS

This study was supported by the National Research Foundation of Korea (NRF), funded by the Ministry of Science, ICT and Future Planning, Korea (2013M3A9B6046418), the National Research Council of Science and Technology [DRC-14-3-KBSI and the Creative Allied Project (CAP)], the Korea Basic Science Institute (C36705), and the National Research Foundation of Korea (NRF) Grant (NRF-2015R1D1A3A01019056 to E. Ha).

DISCLOSURES

No conflicts of interest, financial or otherwise, are declared by the author(s).

AUTHOR CONTRIBUTIONS

Author contributions: J.J., T.K.H., J.L., Y.L., M.N., and D.L. performed experiments; J.J., T.K.H., and J.L. analyzed data; J.J., T.K.H., J.L., C.W.l.R., D.H.R., E.H., and G.-S.H. interpreted results of experiments; J.J. and J.L. prepared figures; J.J., E.H., and G.-S.H. drafted manuscript; J.L., C.W.l.R., D.H.R., E.H., and G.-S.H. edited and revised manuscript; E.H. and G.-S.H. conception and design of research; G.-S.H. approved final version of manuscript.

REFERENCES

1. **Argaud D, Roth H, Wiernsperger N, Leverve XM.** Metformin decreases gluconeogenesis by enhancing the pyruvate kinase flux in isolated rat hepatocytes. *Eur J Biochem* 213: 1341–1348, 1993.
2. **Bell LN, Temm CJ, Saxena R, Vuppalanchi R, Schauer P, Rabinovitz M, Krasinskas A, Chalasani N, Mattar SG.** Bariatric surgery-induced weight loss reduces hepatic lipid peroxidation levels and affects hepatic cytochrome P-450 protein content. *Ann Surg* 251: 1041–1048, 2010.
3. **Berg JM, Tymoczko JL, Stryer L.** Nucleotide biosynthesis. In: *Biochemistry*. Freeman WH, 2002.
4. **Bergman Lilly lecture 1989 RN.** Toward physiological understanding of glucose tolerance. Minimal-model approach. *Diabetes* 38: 1512–1527, 1989.
5. **Buchwald H, Avidor Y, Braunwald E, Jensen MD, Pories W, Fahrbach K, Schoelles K.** Bariatric surgery: a systematic review and meta-analysis. *JAMA* 292: 1724–1737, 2004.
6. **Buchwald H, Estok R, Fahrbach K, Banel D, Jensen MD, Pories WJ, Bantle JP, Sledge I.** Weight and type 2 diabetes after bariatric surgery: systematic review and meta-analysis. *Am J Med* 122: 248–256. e5, 2009.
7. **Cuskelly GJ, Stacpoole PW, Williamson J, Baumgartner TG, Gregory JF 3rd.** Deficiencies of folate and vitamin B_6 exert distinct effects on homocysteine, serine, and methionine kinetics. *Am J Physiol Endocrinol Metab* 281: E1182–E1190, 2001.
8. **de Boer IH, Rue TC, Hall YN, Heagerty PJ, Weiss NS, Himmelfarb J.** Temporal trends in the prevalence of diabetic kidney disease in the United States. *JAMA* 305: 2532–2539, 2011.
9. **Deshpande AD, Harris-Hayes M, Schootman M.** Epidemiology of diabetes and diabetes-related complications. *Phys Ther* 88: 1254–1264, 2008.
10. **Dixon JB, O'Brien PE, Playfair J, Chapman L, Schachter LM, Skinner S, Proietto J, Bailey M, Anderson M.** Adjustable gastric banding and conventional therapy for type 2 diabetes: a randomized controlled trial. *JAMA* 299: 316–323, 2008.
11. **Hardie DG.** Minireview: the AMP-activated protein kinase cascade: the key sensor of cellular energy status. *Endocrinology* 144: 5179–5183, 2003.
12. **Hartley DP, Ruth JA, Petersen DR.** The hepatocellular metabolism of 4-hydroxynonenal by alcohol dehydrogenase, aldehyde dehydrogenase, and glutathione S-transferase. *Arch Biochem Biophys* 316: 197–205, 1995.
13. **Ikramuddin S, Korner J, Lee WJ, Connett JE, Inabnet WB, Billington CJ, Thomas AJ, Leslie DB, Chong K, Jeffery RW, Ahmed L, Vella A, Chuang LM, Bessler M, Sarr MG, Swain JM, Laqua P, Jensen MD, Bantle JP.** Roux-en-Y gastric bypass vs intensive medical management for the control of type 2 diabetes, hypertension, and hyperlipidemia: the Diabetes Surgery Study randomized clinical trial. *JAMA* 309: 2240–2249, 2013.
14. **Jacobs RL, Stead LM, Brosnan ME, Brosnan JT.** Hyperglucagonemia in rats results in decreased plasma homocysteine and increased flux through the transsulfuration pathway in liver. *J Biol Chem* 276: 43740–43747, 2001.
15. **Kannel WB, McGee DL.** Diabetes and cardiovascular disease: the Framingham study. *JAMA* 241: 2035–2038, 1979.
16. **Laferrere B, Reilly D, Arias S, Swerdlow N, Gorroochurn P, Bawa B, Bose M, Teixeira J, Stevens RD, Wenner BR, Bain JR, Muehlbauer MJ, Haqq A, Lien L, Shah SH, Svetkey LP, Newgard CB.** Differential metabolic impact of gastric bypass surgery versus dietary intervention in obese diabetic subjects despite identical weight loss. *Sci Transl Med* 3: 80re2, 2011.
17. **Lamarre SG, Morrow G, Macmillan L, Brosnan ME, Brosnan JT.** Formate: an essential metabolite, a biomarker, or more? *Clin Chem Lab Med* 51: 571–578, 2013.
18. **Lamarre SG, Molloy AM, Reinke SN, Sykes BD, Brosnan ME, Brosnan JT.** Formate can differentiate between hyperhomocysteinemia due to impaired remethylation and impaired transsulfuration. *Am J Physiol Endocrinol Metab* 302: E61–E67, 2012.
19. **Leverve XM, Guigas B, Detaille D, Batandier C, Koceir EA, Chauvin C, Fontaine E, Wiernsperger NF.** Mitochondrial metabolism and type-2 diabetes: a specific target of metformin. *Diabetes Metab* 29: 6S88–6S94, 2003.
20. **Lindenbaum J, Savage DG, Stabler SP, Allen RH.** Diagnosis of cobalamin deficiency. II. Relative sensitivities of serum cobalamin, methylmalonic acid, and total homocysteine concentrations. *Am J Hematol* 34: 99–107, 1990.
21. **Massillon D, Chen W, Barzilai N, Prus-Wertheimer D, Hawkins M, Liu R, Taub R, Rossetti L.** Carbon flux via the pentose phosphate pathway regulates the hepatic expression of the glucose-6-phosphatase and phosphoenolpyruvate carboxykinase genes in conscious rats. *J Biol Chem* 273: 228–234, 1998.
22. **Mehta JL, Rasouli N, Sinha AK, Molavi B.** Oxidative stress in diabetes: a mechanistic overview of its effects on atherogenesis and myocardial dysfunction. *Int J Biochem Cell Biol* 38: 794–803, 2006.
23. **Menendez JA, Joven J.** One-carbon metabolism: an aging-cancer crossroad for the gerosuppressant metformin. *Aging (Albany NY)* 4: 894–898, 2012.
24. **Mingrone G, Panunzi S, De Gaetano A, Guidone C, Iaconelli A, Leccesi L, Nanni G, Pomp A, Castagneto M, Ghirlanda G, Rubino F.** Bariatric surgery versus conventional medical therapy for type 2 diabetes. *N Engl J Med* 366: 1577–1585, 2012.
25. **Morton GJ.** Hypothalamic leptin regulation of energy homeostasis and glucose metabolism. *J Physiol* 583: 437–443, 2007.
26. **Mosharov E, Cranford MR, Banerjee R.** The quantitatively important relationship between homocysteine metabolism and glutathione synthesis by the transsulfuration pathway and its regulation by redox changes. *Biochemistry* 39: 13005–13011, 2000.
27. **Moyer MW.** New insight on bariatric surgery difficult to swallow. *Nat Med* 18: 184–185, 2012.

28. **Mutch DM, Fuhrmann JC, Rein D, Wiemer JC, Bouillot JL, Poitou C, Clément K.** Metabolite profiling identifies candidate markers reflecting the clinical adaptations associated with Roux-en-Y gastric bypass surgery. *PLoS One* 4: e7905, 2009.
29. **Nieman KM, Rowling MJ, Garrow TA, Schalinske KL.** Modulation of methyl group metabolism by streptozotocin-induced diabetes and all-trans-retinoic acid. *J Biol Chem* 279: 45708–45712, 2004.
30. **Ouyang J, Parakhia RA, Ochs RS.** Metformin activates AMP kinase through inhibition of AMP deaminase. *J Biol Chem* 286: 1–11, 2011.
31. **Pastore A, Federici G, Bertini E, Piemonte F.** Analysis of glutathione: implication in redox and detoxification. *Clin Chim Acta* 333: 19–39, 2003.
32. **Porte D Jr.** Banting lecture 1990. Beta-cells in type II diabetes mellitus. *Diabetes* 40: 166–180, 1991.
33. **Rask-Madsen C, Kahn CR.** Tissue-specific insulin signaling, metabolic syndrome, and cardiovascular disease. *Arterioscler Thromb Vasc Biol* 32: 2052–2059, 2012.
34. **Rubino F, Forgione A, Cummings DE, Vix M, Gnuli D, Mingrone G, Castagneto M, Marescaux J.** The mechanism of diabetes control after gastrointestinal bypass surgery reveals a role of the proximal small intestine in the pathophysiology of type 2 diabetes. *Ann Surg* 244: 741–749, 2006.
35. **Savage DG, Lindenbaum J, Stabler SP, Allen RH.** Sensitivity of serum methylmalonic acid and total homocysteine determinations for diagnosing cobalamin and folate deficiencies. *Am J Med* 96: 239–246, 1994.
36. **Savage DB, Petersen KF, Shulman GI.** Disordered lipid metabolism and the pathogenesis of insulin resistance. *Physiol Rev* 87: 507–520, 2007.
37. **Schalinske KL, Smazal AL.** Homocysteine imbalance: a pathological metabolic marker. *Adv Nutr* 3: 755–762, 2012.
38. **Schauer PR, Kashyap SR, Wolski K, Brethauer SA, Kirwan JP, Pothier CE, Thomas S, Abood B, Nissen SE, Bhatt DL.** Bariatric surgery versus intensive medical therapy in obese patients with diabetes. *N Engl J Med* 366: 1567–1576, 2012.
39. **Seyfried F, Li JV, Miras AD, Cluny NL, Lannoo M, Fenske WK, Sharkey KA, Nicholson JK, le Roux CW, Holmes E.** Urinary phenotyping indicates weight loss-independent metabolic effects of Roux-en-Y gastric bypass in mice. *J Proteome Res* 12: 1245–1253, 2013.
40. **Shevchenko A, Wilm M, Vorm O, Mann M.** Mass spectrometric sequencing of proteins from silver-stained polyacrylamide gels. *Anal Chem* 68: 850–858, 1996.
41. **Sjöström L, Lindroos AK, Peltonen M, Torgerson J, Bouchard C, Carlsson B, Dahlgren S, Larsson B, Narbro K, Sjöström CD, Sullivan M, Wedel H.** Swedish Obese Subjects Study Scientific Group. Lifestyle, diabetes, and cardiovascular risk factors 10 years after bariatric surgery. *N Engl J Med* 351: 2683–2693, 2004.
42. **Stenesen D, Suh JM, Seo J, Yu K, Lee KS, Kim JS, Min KJ, Graff JM.** Adenosine nucleotide biosynthesis and AMPK regulate adult life span and mediate the longevity benefit of caloric restriction in flies. *Cell Metab* 17: 101–112, 2013.
43. **Want EJ, Masson P, Michopoulos F, Wilson ID, Theodoridis G, Plumb RS, Shockcor J, Loftus N, Holmes E, Nicholson JK.** Global metabolic profiling of animal and human tissues via UPLC-MS. *Nat Protocols* 8: 17–32, 2013.
44. **Zhang H, DiBaise JK, Zuccolo A, Kudrna D, Braidotti M, Yu Y, Parameswaran P, Crowell MD, Wing R, Rittmann BE, Krajmalnik-Brown R.** Human gut microbiota in obesity and after gastric bypass. *Proc Natl Acad Sci USA* 106: 2365–2370, 2009.
45. **Zinck JW, MacFarlane AJ.** Approaches for the identification of genetic modifiers of nutrient dependent phenotypes: examples from folate. *Front Nutr* 1: 2014.